Journal of
Micro/Nanolithography,
MEMS, and MOEMS

Nanolithography.SPIEDigitalLibrary.org

Cantilever type radio frequency microelectromechanical systems shunt capacitive switch design and fabrication

Kaan Demirel
Erdem Yazgan
Şimşek Demir
Tayfun Akın

SPIE.

Cantilever type radio frequency microelectromechanical systems shunt capacitive switch design and fabrication

Kaan Demirel,[a,b,*] Erdem Yazgan,[a,c] Şimşek Demir,[b] and Tayfun Akın[b,d]
[a]Hacettepe University, Department of Nanotechnology and Nanomedicine, Beytepe, Ankara 06800, Turkey
[b]Middle East Technical University, Department of Electrical and Electronics Engineering, Çankaya, Ankara 06800, Turkey
[c]TED University, Department of Electrical and Electronics Engineering, Çankaya, Ankara 06420, Turkey
[d]Middle East Technical University, MEMS Research and Application Center, Eskisehir Yolu, Ankara 06520, Turkey

Abstract. A new cantilever type radio frequency microelectromechanical systems (RF MEMS) shunt capacitive switch design and fabrication is presented. The mechanical, electromechanical, and electromagnetic designs are carried out to get <40 V actuation voltage, high isolation, and low insertion loss for 24 and 35 GHz and the fabrication is carried out for 24 GHz RF MEMS switch. The fabricated switch shows lower than 0.35 dB insertion loss up to 40 GHz and greater than 20 dB isolation at 22 to 29 GHz frequency band. An insignificant change is observed on RF performance at 24 GHz ($\Delta S_{11} = 1$ dB, $\Delta S_{21} < 0.1$ dB) after 200°C thermal treatment for 30 min. The switch is fabricated on quartz wafer using an in-house surface micromachining process with amorphous silicon sacrificial layer structure. Total MEMS bridge thickness is aimed to be 4 μm and consists of 2-μm-thick sputtered and 2-μm-thick electroplated gold layers. The bridge bending models and pull-down voltage simulations are carried out for different stress levels and equivalent Young's modulus (E_{avg}). [DOI: 10.1117/1.JMM.14.3.035005]

Keywords: amorphous silicon; buckling; radio frequency microelectromechanical systems; thermal treatment; sacrificial layer; stress; temperature.

Paper 15082 received May 19, 2015; accepted for publication Aug. 20, 2015; published online Sep. 21, 2015.

1 Introduction

Radio frequency microelectromechanical system (RF MEMS) switches have several performance advantages, such as high isolation,[1] very low loss,[2] and low-power consumption with respect to conventional diodes. Generally, RF MEMS switches have cantilever type[3,4] or fixed–fixed type[5,6] bridge structures. These two structures have different advantages and disadvantages with respect to each other. In the sense of the biaxial inplane compressive stress, the fixed–fixed beam bridges buckle when the critical stress is exceeded.[7,8] Furthermore, the inplane stress on the cantilever structure is released at the free end of the cantilever. Also, the cantilever structure is very sensitive to the stress gradient in the thickness axis and bends upward or downward but the bending can be reduced by using shorter cantilever structures.[9] Therefore, the vertical stress gradient on cantilever structures must be controlled carefully to avoid unexpected bending on the long cantilever structures.

Another important point is the temperature effects on the MEMS bridges. The temperature-dependent expansion increases the compressive stress level on the fixed–fixed beam and can cause permanent deformation on the MEMS bridge. The single-layer cantilever type MEMS bridge extends with increasing temperature, releases the stress on the bridge, and returns to its original position after decreasing the temperature. Generally, actuation voltage of the cantilever type switches is lower than that of the fixed–fixed type switches due to their low spring constant values, but low spring constant fixed–fixed bridge structures[10] can be designed as well. The critical point of the design is to consider the tradeoff between the stress durability and actuation voltage.

Usually, RF MEMS switches are fabricated on a single substrate. These RF MEMS switches must be packaged using hermetic or near-hermetic seals to protect them from moisture, dust particles, and other environmental effects. Generally, the packaging temperature processes of the MEMS devices is very high (≥190°C). Because the typical RF MEMS switch has suspended thin bridge structure, packaging temperature can lead to deformation on the MEMS bridges. The fixed–fixed beam type RF MEMS bridges suffer from compressive effects of the high packaging temperatures. Because the cantilever type MEMS bridges are fixed at one end, these structures have more tolerance to compressive effects of temperature than fixed–fixed type bridges.

In this work, cantilever type RF MEMS shunt capacitive switches are designed for 24 and 35 GHz radar applications. The fabrication is carried out for 24-GHz switch structure. In addition, the inductive tuning for adjusting isolation frequency is explained. The isolation frequency tuning is carried out by adding inductive region on coplanar waveguide (CPW) before and after MEMS bridge structure. The mechanical, electromechanical, and RF models are carried out by using COMSOL Multiphysics modeling software. In the mechanical modeling study, the MEMS bridge is divided into two layers. The bottom layer is modeled as sputtered Au layer and the top layer is modeled as electroplated Au layer. The stress-dependent bending model is performed by defining the residual stresses on each layer. To measure the sputtered Au layer stress, a 2-μm-thick Au layer was

*Address all correspondence to: Kaan Demirel, E-mail: kdemirel@mems.metu.edu.tr

1932-5150/2015/$25.00 © 2015 SPIE

deposited on the 4-in. Si wafer by using sputter system and the residual stress was measured by using FLX 2320-S stress measurement system and found as 20 ± 1 MPa (tensile). This stress was set as sputtered Au layer stress (σ_1) in the bending model. We know that the residual stress of the electroplated Au changes from 40 to 50 MPa tensile for our in-house deposition conditions. The electroplated Au layer residual stress (σ_2) was set from 30 to 50 MPa for the stress-dependent bending model. Because the mechanical properties of a thin film depends on the deposition process, the Young's modulus of sputtered and electroplated Au layers can be different from each other.[11,12] Therefore, the equivalent Young's modulus (E_{avg}) for two layer cantilever structure, which consists of sputtered and electroplated Au layers, is used and set from 55 to 70 GPa. The actuation voltages were estimated for different σ_2 and E_{avg} values and these values were compared with measurement results. MEMS bridge spring constant and actuation voltage dependency on the mechanical arm length of the cantilever were investigated to get aimed actuation voltage value (<40 V).

The fabrication is carried out for 24 GHz RF MEMS switch. The fabrication process is developed at the Middle East Technical University (METU)-MEMS Research and Application Center. The CPW structure is fabricated by using sputtered gold layer. The plasma enhanced chemical vapor deposition (PECVD) Si_xN_y is selected as a dielectric layer. An amorphous silicon (a-Si) sacrificial layer is used with SiO_x diffusion barrier (between Au and a-Si). MEMS bridge thickness is targeted at 4 μm but it varies from 3.5 to 4 μm due to the electroplated Au layer nonuniformities. Therefore, the fabricated bridge structure consists of 2-μm-thick sputtered gold and 1.5- to 2-μm-thick electroplated gold layers.

The pull-down voltage and RF measurements were performed and the equivalent parallel gap (effective bridge height) is estimated by fitting the RF measurements and RF simulation results. This fitting procedure was done by sweeping the bridge height in the simulation to get equal upstate S_{11} pattern with the measured S_{11} pattern. It should be noted that this method is just an approximation to estimate the equivalent parallel gap between the signal line and bridge. On the other hand, the upstate S_{11} performance of the switch depends on the distance between the signal line and ground line on the coplanar waveguide (CPW). An over etching of the metals during the CPW fabrication changes the signal to ground distance and affects S_{11} pattern.

2 Radio Frequency Microelectromechanical System Switch Design

The cantilever type RF MEMS capacitive shunt bridge structure was designed with two mechanical arms and a capacitive area. The mechanical arms are fixed onto the ground line of the CPW to get an electrical contact. Generally, cantilever type bridges are used for DC-contact series RF MEMS switch designs, and fixed–fixed beam bridges are used for RF MEMS capacitive shunt switches with different geometries.[13,14] A typical fixed–fixed beam structure suffers from high temperatures during the packaging process. The compressive stress on the fixed–fixed beam increases with increasing temperature. Therefore, the beam structure buckles at high temperatures and permanently deforms due to the increased stress at the anchor points. The main advantage of the cantilever type structure is the temperature tolerance with respect to fixed–fixed beams. The cantilever structure expands in the structure plane with increasing temperature and returns to its original position after decreasing temperature. In this study, cantilever bridge structure was designed for RF MEMS shunt capacitive switch. The actuation voltage dependency on the mechanical arm length and residual stresses of MEMS bridge was investigated by using COMSOL Multiphysics modeling software. The fabrication of the MEMS bridge was made using sputtered and electroplated Au layers. Because of the dependency of material properties (such as Young's modulus, thermal expansion coefficient) on the fabrication process, the cantilever bridge was modeled as a multilayer structure with an equivalent Young's modulus. The equivalent Young's modulus of multilayer structures can be calculated by using Eq. (1):[15]

$$E_{\text{avg}} = \frac{\sum E_i t_i}{\sum t_i}, \tag{1}$$

where, E_i and t_i are the Young's modulus and the thickness of the i'th layer. Residual stress-based bending model and the pull-down voltage calculations were performed by using different equivalent Young's modulus ($E_{\text{avg}} = 55$ to 70 GPa with 5 GPa step).

In this study, the RF designs were carried out to get high isolation from 24 to 35 GHz with different inductive tuning sections without capacitive area and bridge dimension changing. Moreover, considering this design, the capacitive area of the MEMS bridge can be changed to adjust the down-state capacitance to get high isolation at desired frequency. Figure 1 and Table 1 show the MEMS bridge dimensions for 24 and 35 GHz designs with different capacitive areas. The main difference in these two designs is capacitive area. The c_2 dimension is changed for this purpose.

The spring constant of this cantilever structure depends on the mechanical arm length (c_1). To find the spring constant for different c_1 values, a 100 Pa pressure was applied on the capacitive area (Fig. 1). Next, the maximum deflections on

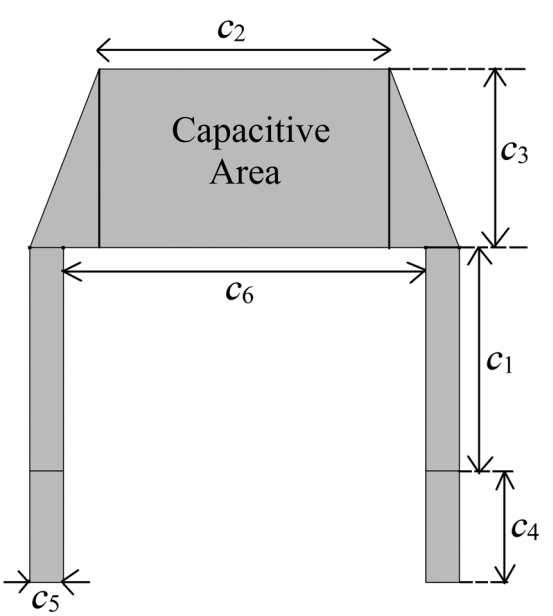

Fig. 1 Microelectromechanical systems (MEMS) bridge dimension labels.

Table 1 Microelectromechanical systems bridge dimensions.

Label	Dimension (μm) for 24 GHz	Dimension (μm) for 35 GHz
Mechanical arm length, c_1	50 to 100	50 to 100
Capacitive area width, c_2	130	100
Capacitive area length, c_3	80	80
Anchor width, c_4	50	50
Mechanical arm width, c_5	15	15
Mechanical arm distance, c_6	162	132

the MEMS bridge for different mechanical arm lengths under this pressure were simulated and the corresponding force was divided by these maximum deflection values to find the spring constant of the bridge. Then, these spring constant values were used in analytical pull-down voltage calculations. It should be noted that the spring constant and pull-down voltage of the switch are proportional to t^3 and $t^{3/2}$, respectively. Therefore, the thickness of the bridge is very important to obtain the desired pull-down voltage. Figures 2(a) and 2(b) show the spring constant dependency on bridge thickness and Young's modulus. The spring constant increases from 23 to 34 N/m by increasing the bridge thickness from 3.5 to 4 μm for 50-μm mechanical arm length and $E_{avg} = 60$ GPa. Another important point is the Young's modulus of the bridge material. The 4-μm-thick designed bridge structure has 40 and 31.4 N/m spring constant for $E_{avg} = 70$ GPa and $E_{avg} = 55$ Gpa, respectively, for $c_1 = 50$ μm. This difference between the spring constants (k) comes from the direct proportionality between the k and E. On the other hand, the Young's modulus of the bridge affects the actuation voltage because the proportionality of $V_P \alpha E^{1/2}$.

The cantilever type MEMS bridge bends upward or downward due to the vertical stress gradient. The typical cantilever structure bending value depends on the stress gradient ($\Delta\sigma$), length of the cantilever (L), effective Young's modulus [$E_e = 1/(1-v^2)$, v is Poisson's ratio] and given by Eq. (2):[16]

$$\delta = \frac{\Delta\sigma L^2}{2E_e}. \tag{2}$$

Average residual stresses of the sputtered and electroplated Au layers were measured before buckling modeling. A 2-μm-thick sputtered Au layer (on Si) average residual stress was measured as 20 MPa tensile (σ_1), and a 2-μm-thick electroplated Au layer (on Si with Au seed layer) average residual stress is measured as 40 to 50 MPa tensile (σ_2). These residual stress values were defined in the model to estimate stress gradient-based bending on the MEMS bridge.

Figure 3 shows the maximum bending on the MEMS bridge under the condition of $T = 20$°C, $\sigma_1 = 20$ MPa, $\sigma_2 = 45$ MPa, and $E_{avg} = 60$ GPa for different mechanical arm length and thickness of the MEMS bridge. The maximum deflections on the 3.5-μm-thick bridge are 1.58 and 0.8 μm for $c_1 = 100$ μm and $c_1 = 50$ μm, respectively. Similarly, the maximum deflection on the 3.5-μm-thick bridge are 1.42 μm and 0.73 μm for $c_1 = 100$ μm and $c_1 = 50$ μm, respectively.

As shown in Fig. 3, the deflection on the outer point [Fig. 3(d)] is more than that of the inner point. Figure 4(a) shows the inner and outer point deflections with respect to mechanical arm length for different σ_2 values. The deflections on these points decrease by decreasing the mechanical arm length. It is an expected result because the maximum deflection depends on the cantilever length according to Eq. (2). Figure 4(b) shows the cantilever edge profile for different c_1 and σ_2 values. It is seen that the maximum deflection decreases by decreasing the c_1 and σ_2 values, as expected.

If the bridge width (c_2) is large, the stress difference between the Au layers causes a transverse bending on the MEMS bridge. Therefore, the deflections of the inner and outer points are different from each other. The difference between the inner and outer points increases by increasing c_2 width as shown in Fig. 5(a). It should be noted that the c_2 width must be chosen to get required capacitance for RF isolation at desired frequency. In this study, c_2 was chosen as 130 μm for 24 GHz isolation frequency. The maximum deflection on the cantilever type bridge was calculated analytically by using Eq. (2) and it was compared with simulation results. The analytical calculation was carried out by using E_e with the Au Poisson's ratio of 0.44. Figure 5(b) shows the analytical calculation and simulation results of the maximum deflection on the cantilever bridge for different E_{avg} and σ_2 values. As can be seen, the results are in close agreement for $E_{avg} = 55$, 60, 65, 70 GPa and $\sigma_2 = 30$, 35, 40, 45, 50 MPa ($t = 3.5$ μm). The deflection

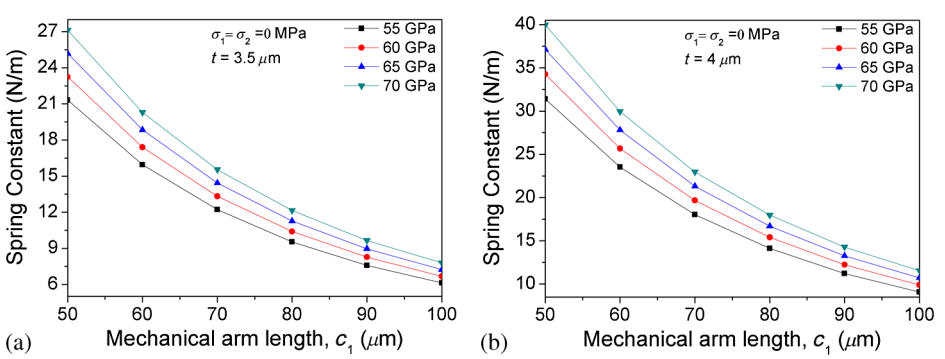

Fig. 2 Different mechanical arm length (c_1) and corresponding spring constant values of (a) 3.5-μm-thick bridge and (b) 4-μm-thick bridge for $E_{avg} = 55$, 60, 65, 70 GPa ($\sigma_1 = \sigma_2 = 0$ MPa).

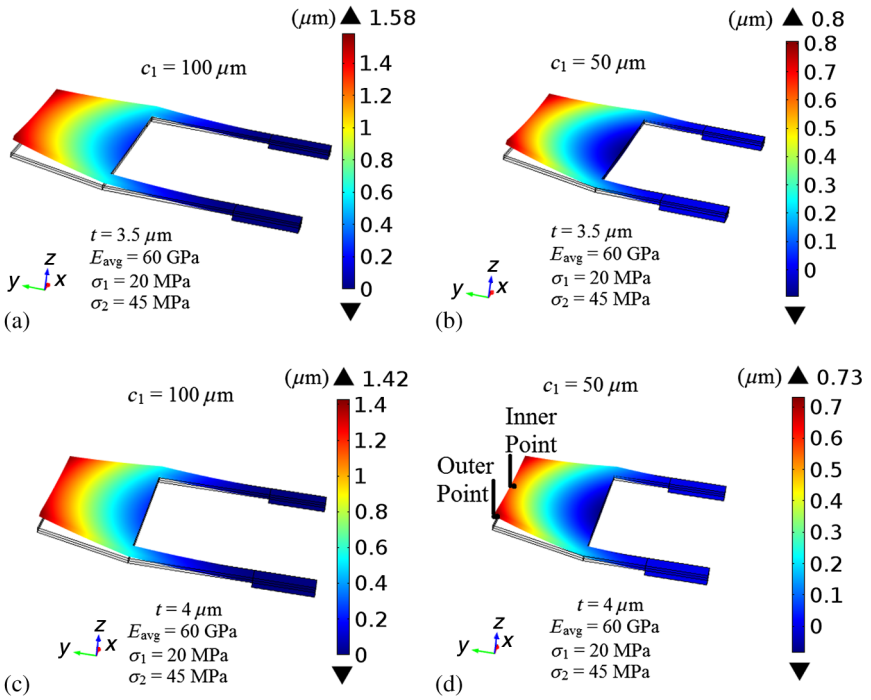

Fig. 3 MEMS bridge bending model for different mechanical arm length of 24 GHz RF MEMS switch, (a) $c_1 = 100\ \mu$m ($t = 3.5\ \mu$m), (b) $c_1 = 50\ \mu$m ($t = 3.5\ \mu$m), (c) $c_1 = 100\ \mu$m ($t = 4\ \mu$m), (d) $c_1 = 50\ \mu$m ($t = 4\ \mu$m; $T = 20°$C, $E_{avg} = 60$ GPa, $\sigma_1 = 20$ MPa, $\sigma_2 = 45$ MPa).

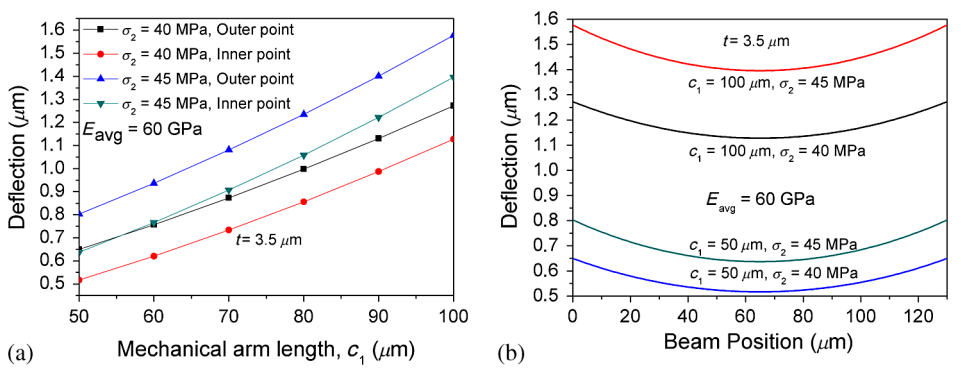

Fig. 4 (a) Inner and outer point deflection of the MEMS bridge and (b) edge profile illustration of the MEMS bridge for $E_{avg} = 60$ GPa and $\sigma_2 = 40$ and 45 MPa ($t = 3.5\ \mu$m).

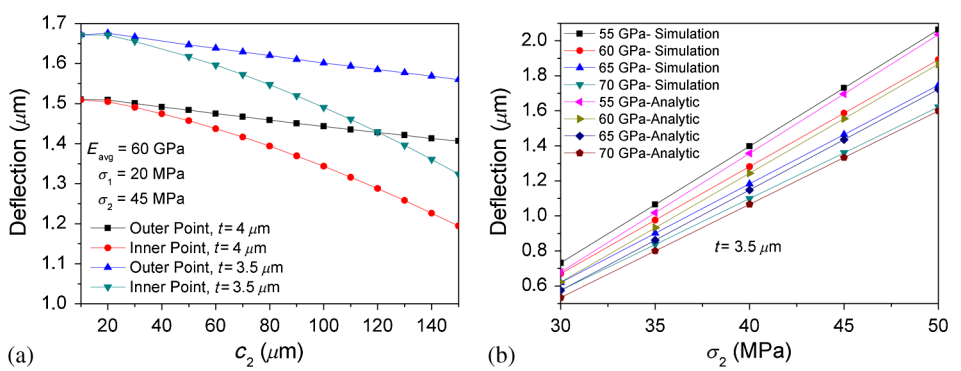

Fig. 5 (a) Inner and outer point deflection values of the MEMS bridge ($E_{avg} = 60$ GPa, $\sigma_1 = 20$ MPa, $\sigma_2 = 45$ MPa, $t = 3.5, 4\ \mu$m). (b) Analytic and simulated values of maximum deflection on the MEMS bridge for $E_{avg} = 55$, 60, 65, 70 GPa and $\sigma_1 = 20$ MPa, $\sigma_2 = 30$, 35, 40, 45, 50 MPa ($t = 3.5\ \mu$m).

at the edge of the bridge increases by the decreasing of the equivalent Young's modulus of the bridge, as expected.

The electroplated Au layer stress level affects the cantilever bridge bending level [Fig. 5(b)]. The stress gradient ($\Delta\sigma$) across the bridge thickness increases by increasing upper layer (electroplated layer) stress (σ_2). As shown, the bending on the cantilever MEMS bridge is very sensitive to the stress gradient in the thickness axis. The maximum bending on the bridge increases from 0.7 to 1.9 μm by increasing σ_2 from 30 to 50 MPa, respectively, for $E_{avg} = 60$ GPa, $t = 3.5$ μm.

The actuation voltage of the RF MEMS switch is aimed at <40 V for this study. The actuation voltage (V_p) can be calculated by using Eq. (3):[15]

$$V_p = V\left(\frac{2g_0}{3}\right) = \sqrt{\frac{8kg_0^3}{27\varepsilon_0 W w}}, \tag{3}$$

where k is the spring constant, $g_0 = 2$ μm ($\sigma_1 = \sigma_2 = 0$ MPa) is the bridge height, $W = 130$ μm and $w = 80$ μm are actuation electrode dimensions (Fig. 6), and ε_0 is the permittivity of free space.

Figure 7(a) shows the analytically calculated pull-down voltages (V_p) for different c_1, E_{avg} and $\sigma_1 = \sigma_2 = 0$ MPa (unbended bridge). Also, the pull-down voltages of the stressed bridge ($\sigma_1 = 20$ MPa, $\sigma_2 = 45$ MPa, bended bridge) for $E_{avg} = 60$ GPa and $c_1 = 50$, 80, 100 μm were simulated.

As seen in Fig. 7(a), a vertical stress gradient on the MEMS bridge results in increased actuation voltage (V_p). V_p values increase from 13 V ($\sigma_1 = \sigma_2 = 0$ MPa) to 23.5 V ($\sigma_1 = 20$ MPa, $\sigma_2 = 45$ MPa) and from 24.5 V ($\sigma_1 = \sigma_2 = 0$ MPa) to 31.5 V ($\sigma_1 = 20$ MPa, $\sigma_2 = 45$ MPa) for $c_1 = 100$ μm and $c_1 = 50$ μm, respectively (for $E_{avg} = 60$ GPa, $t = 3.5$ μm). This is a result of vertical stress gradient-based bended bridge. Figure 7(b) shows that the analytical and numerical solutions of the pull-down voltages are in close agreement for different E_{avg} and c_1 values ($\sigma_1 = \sigma_2 = 0$ MPa, $t = 4$ μm).

The pull-down voltage was simulated by finding the required voltage value to hold the end edge of the cantilever bridge at a preset height. During the simulation, the preset height was swept with 0.1-μm step and the corresponding required voltage was observed. It should be noted that the maximum difference between the analytically and numerically calculated pull-down voltages at $c_1 = 50$ μm is 0.5 V. The simulation can be carried out more accurately by decreasing the sweep step of the preset height of the bridge and increasing the mesh number of the simulation.

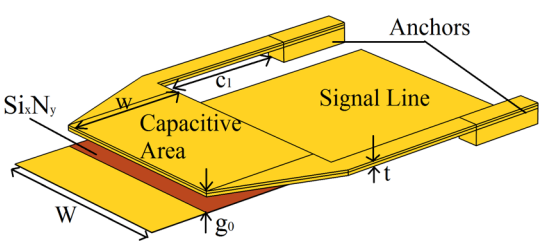

Fig. 6 Capacitive area and MEMS bridge actuation electrode dimensions.

3 Fabrication

In this study, a 24-GHz RF MEMS cantilever shunt capacitive switch was fabricated on quartz wafer using an in-house process developed at the METU-MEMS Research and Application Center. Figure 8 shows the cross-sectional view of fabrication steps. The summarized process steps are given below:

i. Ti/Au CPW and Si_xN_y dielectric deposition and etching.
ii. SiO_x/a − Si/SiO_x sacrificial layer deposition.
iii. Anchor area opening.
iv. Sputtered gold deposition.
v. Sputtered gold etching and formation of electrical path for electrodeposition.
vi. Gold electrodeposition.
vii. Etching of electrical path.
viii. Releasing the MEMS bridge.

A 1-μm-thick Au layer was deposited on the quartz wafer with 20-nm-thick Ti adhesion layer by using sputter system. CPW structure was formed by etching Au and Ti layers. Next, a 0.3-μm-thick Si_xN_y dielectric film was deposited on the CPW structure by using PECVD. A 2-μm-thick

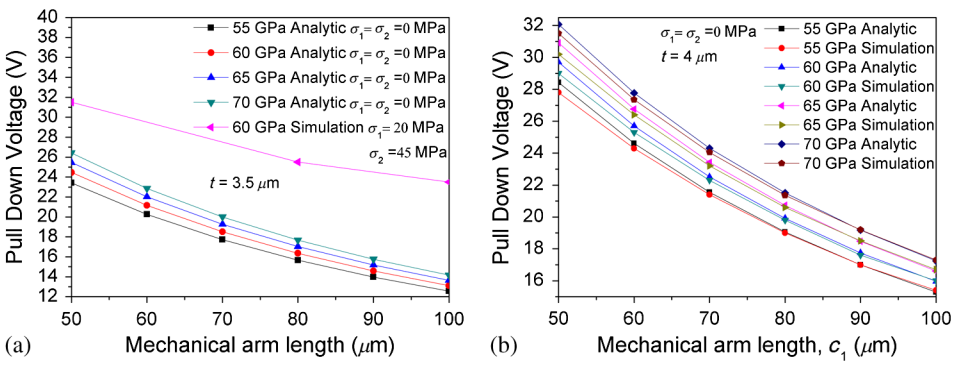

Fig. 7 Analytically calculated and simulation results of MEMS bridge pull-down voltages (a) for $\sigma_1 = \sigma_2 = 0$ MPa, $E_{avg} = 55$, 60, 65, 70 MPa and for $\sigma_1 = 20$ MPa, $\sigma_2 = 45$ MPa, $E_{avg} = 60$ Mpa ($t = 3.5$ μm), (b) for $\sigma_1 = \sigma_2 = 0$ MPa, $E_{avg} = 55$, 60, 65, 70 MPa and different mechanical arm lengths ($t = 4$ μm).

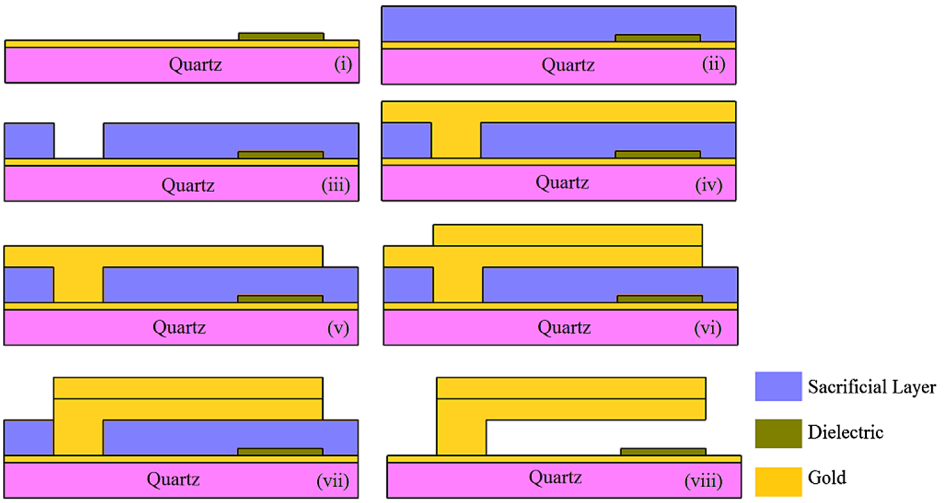

Fig. 8 Fabrication process steps for cantilever type RF MEMS shunt capacitive switch.

PECVD a-Si layer was used as a sacrificial layer. Then, a 30-nm-thick SiO_x layer was deposited before and after a-Si layer as diffusion barrier between the Au and a-Si. The deposited $SiO_x/a-Si/SiO_x$ layers were patterned to define the anchor areas of the MEMS bridge. These $SiO_x/a-Si/SiO_x$ layers can be etched by using buffered hydrofluoric acid (BHF) for SiO_x and deep reactive ion etcher (DRIE) for a-Si etching [Fig. 9(a), method A]. On the other hand, the etching processes can consist of RIE etching for SiO_x and DRIE for a-Si etching [Fig. 9(a), method B].

Because this step of fabrication is an anchor area opening process, the SiO_x layer under the a-Si must not be etched. In this study, $SiO_x/a-Si/SiO_x$ layers were etched by using method B. The top SiO_x layer was opened by RIE etching process and a-Si layer was opened by using DRIE. Next, the bottom SiO_x layer was etched by using RIE. As mentioned previously, the wet BHF etching process could be used for etching of the SiO_x layers at anchor areas. It should be noted that the wet BHF etching process caused swelling on the sacrificial layer due to the penetrating of the HF molecules into the a-Si and etching SiO_x layer under a-Si. In addition, the wet BHF etching process results in an over etched SiO_x profile. Figure 9(b) shows the BHF and plasma etching process of the SiO_x layers. As shown, the plasma etch process is a directional (anisotropic) process. Moreover, fluorine-based plasma does not penetrate though the photoresist and a-Si layers. Therefore, the process-dependent sacrificial layer swelling is not observed.

The wafer was coated with 2-μm-thick sputtered Au layer after the anchor areas opening process. This layer is used as a seed layer for the MEMS bridge structure. The seed layer was patterned to form MEMS bridge structure for $c_1 = 100\ \mu$m. During this process, an electrical path was formed for the electroplating process (Fig. 10).

Then the bridge thickness was increased to 4 μm with a 2-μm-thick electroplated Au layer. Because of the wafer level nonuniformity of the Au electroplating process, the thickness of this layer varies between 1.5 and 2 μm. The electroplating process was optimized to get minimum residual stress on the Au layer. In this process step, a BDT-510 noncyanide gold plating solution was used. The optimized process parameters for gold electroplating are 45°C solution temperature and 3.5 $mA/\mu m^2$ current density. Figure 11(a) shows the released MEMS bridge with nonoptimized electroplating process. The seed layer was etched after the electroplating process.

The wafer was diced into the small parts to release the RF MEMS switches. The MEMS bridge release process was performed by using XeF_2 and vapor hydrofluoric (VHF) etching processes. The a-Si layer was etched by using XeF_2 etching process and then the top and bottom SiO_x diffusion layers were etched by using VHF etching process. The released and stress optimized RF MEMS switch is shown in Fig. 11(b).

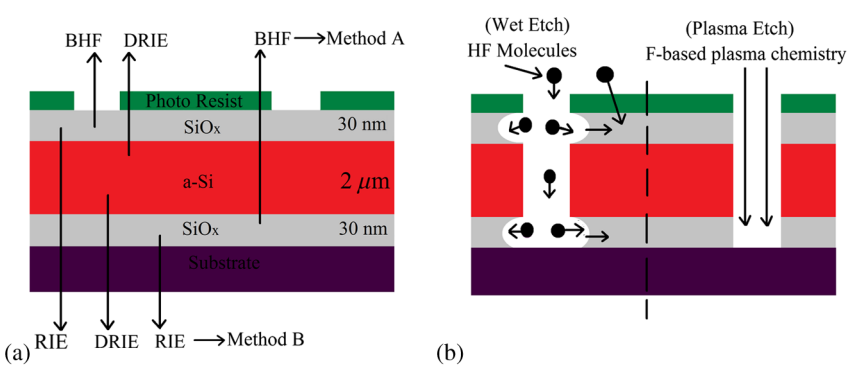

Fig. 9 (a) Sacrificial layer etching methods, (b) wet hydrofluoric acid and plasma etching process comparison.

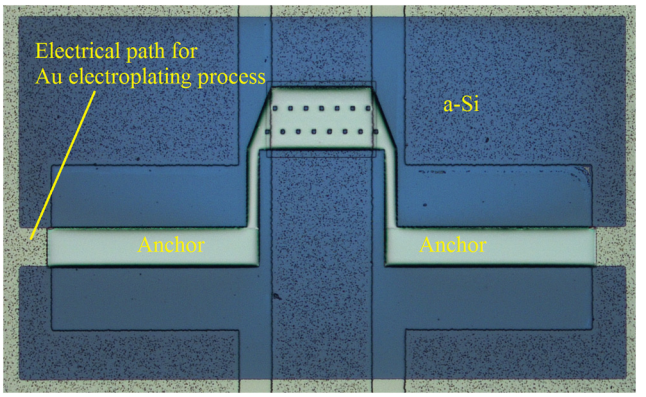

Fig. 10 Electroplated MEMS bridge and electrical path for electroplating process.

4 Measurements

The pull-down and RF measurements were carried out by using Agilent E8361A 10 MHz–67 GHz Network Analyzer, Agilent E6331A DC power supply on a probe station. The pull-down voltages were measured between 24 and 28 V after fabrication. The difference between the pull-down voltage can be attributed to thickness difference between the samples due to nonuniform coating of electroplated Au layer. Table 2 shows the simulated pull-down voltages with expected σ values and different equivalent Young's modulus. The zipping effect and the topological step on the bridge due to the underlayer topology were neglected during the pull-down voltage simulations.

As can be seen from simulation results, the upper layer (electroplated layer) residual stress plays an important role on the bridge bending and influences the actuation voltage. It should be noted that if the cantilever bridge structure consists of two or more layers, the stresses for each layer must be controlled carefully to achieve the desired performance. According to the simulation results, the pull-down voltages vary from 21.5 to 30 V for different t, E_{avg}, σ_1, and σ_2 values (Table 2). In the case of $E_{avg} = 60$ GPa, $\sigma_1 = 20$ MPa and $\sigma_2 = 45$ MPa values, the actuation voltages were simulated at 23.5 and 26.5 V for $t = 3.5$ μm and $t = 4$ μm, respectively. By considering the zipping effect during the measurement, it can be said that these values are in agreement with measured pull-down voltage values. In addition, the switch was annealed at 200°C for 30 min to observe the thermal effects on pull-down voltage. The measured pull-down voltage of annealed switches is higher than that of the unannealed switches and measured between 27 and 32 V. The difference between the pull-down voltages of annealed and unannealed switches can be attributed to temperature-dependent bending and plastic deformation on the bridge.

Normally, a single-layer cantilever structure expands in the bridge plane with increasing temperature and then returns to its original position after decreasing temperature without permanent deformation. The increased pull-down voltage and variation in the upstate S_{11} parameter (explained in RF measurement results) after heat treatment show a permanent deformation on the fabricated bridge. This permanent deformation on the fabricated bridge can be originated from the differences between the thermal expansion coefficients (TEC) of sputtered and electroplated gold layers and

Table 2 Pull-down voltage simulation results for different E_{avg}, σ_1, σ_2, and bridge thicknesses.

E_{avg} (GPa)	σ_2 (MPa)	σ_1 (MPa)	V_{ps} (V) with ±0.5 V accuracy	
			$t = 3.5$ μm	$t = 4$ μm
55	40	20	22	24.5
55	45	20	23.5	26.5
60	40	20	21.5	24.5
60	**45**	**20**	**23.5**	**26.5**
70	45	20	23.5	28
70	50	20	25.5	30

Note: Measured $V_p = 24$ to 28 V (before annealing), $V_p = 27$ to 32 V (after annealing).
Bold Values indicate the best compatible simulation values with the measurement results.

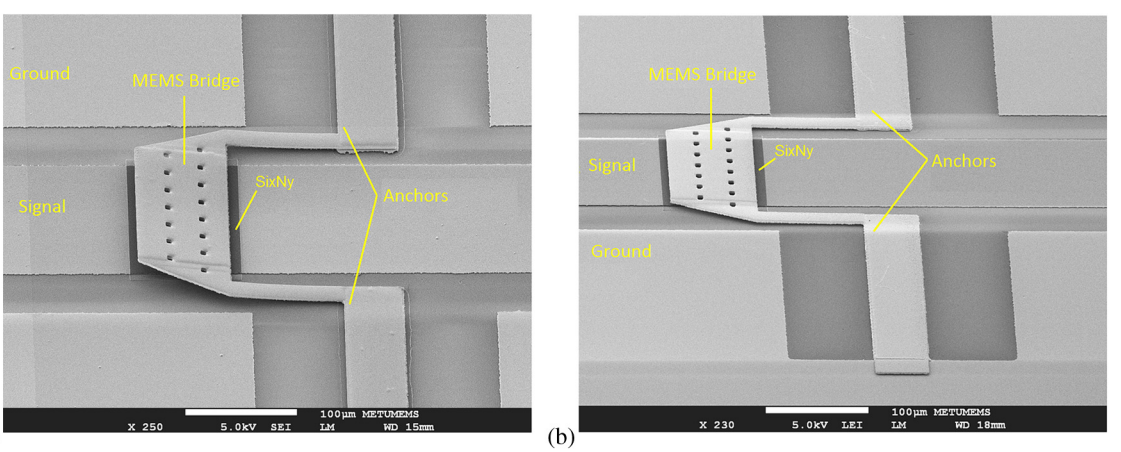

(a) (b)

Fig. 11 (a) Scanning electron microscope (SEM) image of the released 24 GHz RF MEMS switch with nonoptimized electroplating process and (b) SEM image of the released MEMS switch after optimized electroplating process.

rearrangement of the atoms at the intersection between these layers. It is known that the TEC of a material depends on the fabrication process.[17] The other reason can be an undesired deformation at the anchors or on the capacitive area of the bridge at high temperature.

There is no significant change on RF measurement results at 24 GHz (1 dB difference) and aimed pull-down voltage (<40 V) for this study. When this design is compared with the typical fixed–fixed beam structures, the temperature tolerance of this design is an advantage for high temperature packaging process.

Electromagnetic design of the RF MEMS switch was carried out to get low loss and high isolation from 24 to 35 GHz frequency by inductive tuning. The bridge height was designed as 2 μm. The capacitive areas were designed as 130×80 μm^2. The inductive tuning sections were added next to the anchors to adjust the isolation frequency. Figure 12 shows these inductive tuning sections and the MEMS bridge on the CPW structure. By increasing the length of l, the inductance can be increased and the isolation frequency can be decreased to lower frequencies. The mechanical arm length increases the bridge inductance and contributes to total inductance of the switch. This inductance contribution of the mechanical arm length allows getting RF resonance frequency at lower frequencies with short l length. The isolation frequency (resonance frequency) is 35 GHz for $l = 50$ μm and it decreased to 24 GHz by increasing the l length to 200 μm. Additionally, the isolation frequency can be lowered by increasing the downstate capacitance level. It can be achieved using a larger capacitance area or a thinner dielectric layer between the bridge and signal line. The larger capacitive area can cause an undesirable bending on the bridge at high temperatures and the thinner dielectric can cause a failure under applied voltage. Therefore, the mechanical properties of the bridge and the dielectric strength must be considered during the design of a switch with a larger capacitive area and a thinner dielectric layer, respectively.

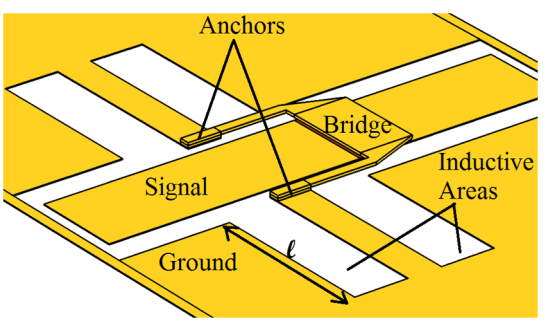

Fig. 12 General view of RF MEMS switch structure and inductive tuning sections.

Figure 13(a) shows the dielectric thickness effects on the isolation frequency and the measured isolation of fabricated switch (less than −30 dB at 24 GHz). As can be seen, the isolation frequency decreases from ~24 to 22.5 GHz by decreasing the dielectric thickness from 0.3 to 0.25 μm. In this study, a 0.3-μm-thick Si_xN_y layer was used as a dielectric layer. Figure 13(b) shows the effects of the length of l on the isolation frequency. The isolation frequency goes beyond the 40 GHz for $l = 0$ μm. In this study, the isolation frequency was adjusted to 24 GHz by using $l = 200$ μm.

The upstate RF simulations is performed for $g_0 = 2$ μm and the S_{11} is found as less than −20 dB at 24 GHz for 24 GHz RF MEMS switch [Fig. 14(a)]. The RF measurements were performed up to 40 GHz at room temperature. The upstate S_{11} was recorded as less than −15 dB up to 40 GHz. Then, the simulation was performed to find the equivalent parallel gap (effective bridge height) for parallel bridge structure (without stress). According to the simulation results, the upstate performance of the RF MEMS switch with 3-μm parallel bridge height is in close agreement with the measurement results [Fig. 14(a)]. The residual stresses on the Au layers result in upward bending on the MEMS bridge. Therefore, the bridge height increases and affects the upstate performance of the switch. A very low insertion loss was measured at 24 GHz [less than −0.25 dB; Fig. 14(b)].

A 200°C and 30 min thermal treatment was applied to the fabricated switch to observe the thermal effects on RF performance. The RF measurements were performed after this thermal treatment and 1-dB difference was observed in upstate S_{11} value at 24 GHz [Fig. 14(a)]. This low difference in S_{11} value can be attributed to low bridge height difference between annealed and unannealed switches. Further, the difference between the upstate S_{21} values of annealed and unannealed switches is lower than 0.1 dB. These results show that the designed 24-GHz cantilever type RF MEMS shunt capacitive switch has more tolerance to high temperature than typical fixed–fixed structures and can be packaged by using our in-house 200°C packaging process.

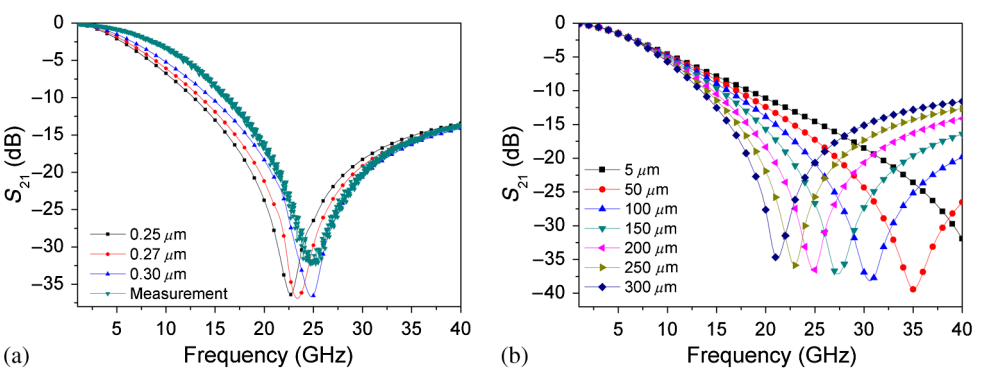

Fig. 13 (a) Dielectric thickness effects on the downstate isolation frequency ($l = 200$ μm) and (b) inductance effects on the downstate isolation frequency.

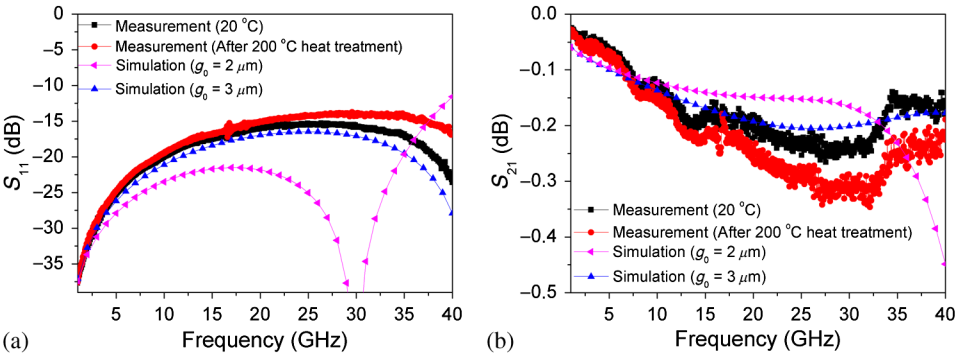

Fig. 14 Measured and simulated S-parameter of 24 GHz RF MEMS switch. (a) The S_{11} measurements and simulation results. The effective bridge height is found as 3 μm before 200°C thermal treatment, (b) S_{21} measurements and simulation results, and (c) isolation of the RF MEMS switch, S_{21}, is better than −25 dB at 24 GHz.

5 Conclusion

In this study, the cantilever type RF MEMS shunt switch design and fabrication are explained. The actuation voltage of this type of RF MEMS switches can be adjusted by changing mechanical arm length. This dimension affects the residual stress-based bridge bending, therefore, the dimensions should be chosen carefully. The downstate capacitive area can be changed easily with this design and the downstate capacitance can be adjusted. The other advantage of this design is the isolation frequency tunability by adjusting the inductive area dimensions without any change to the mechanical design. This design also has the flexibility of the cantilever type structures at high temperatures.

The pull-down voltage of this cantilever type design strongly depends on the bending level of the bridge due to vertical stress gradient. Therefore, the stresses of each layer must be controlled carefully.

The fabricated RF MEMS switch shows very low loss (less than −0.35 dB) in upstate position up to 40 GHz before and after thermal treatment. The residual stresses on the cantilever bridge layers are very important for upstate RF performance because of the cantilever bridge bending under vertical stress gradient. The upstate RF performance can be enhanced by using a thinner sacrificial layer than 2 μm to compensate for increased bridge height due to residual stress on the bridge. A PECVD a-Si sacrificial layer process is a thickness controllable process with high accuracy. Therefore, it is a very suitable material for this adjustment. The switch shows high isolation (less than −20 dB) at 22- to 29-GHz frequency band. Furthermore, this designed and fabricated MEMS bridge structure can be created with a very thin seed layer (<2 μm) of Au and the bridge thickness can be increased by an electroplating process to decrease the cost. This type bridge can be considered as a single layer structure and can be modeled by using stress gradient approximation. In future work, the cantilever type RF MEMS shunt capacitive switch will be fabricated as a fully electroplated bridge and the reliability- and temperature-dependent performance tests will be performed.

Acknowledgments

This work is supported by The Scientific and Technological Research Council of Turkey (Grant No. TUBITAK-109A008). This research was carried out using the computer and process facilities of Middle East Technical University (METU) Electrical and Electronics Engineering Department, and METU-MEMS Research and Application Center. The authors would like to thank Çağrı Çetintepe for his support in the measurements.

References

1. J. B. Muldavin and G. M. Rebeiz, "High-isolation CPW MEMS shunt switches. 1. Modeling," *IEEE Trans. Microwave Theory Tech.* **48**, 1045–1052 (2000).
2. C. L. Goldsmith et al., "Performance of low-loss RF MEMS capacitive switches," *IEEE Microwave Guided Wave Lett.* **8**, 269–271 (1998).
3. N. Nishijima, J. J. Hung, and G. M. Rebeiz, "A low-voltage high contact force RF-MEMS switch," in *IEEE MTT-S Int. Microwave Symposium Digest*, Vol. 2, pp. 577–580 (2004).
4. H. C. Lee et al., "Design, fabrication and RF performances of two different types of piezoelectrically actuated ohmic MEMS switches," *J. Micromech. Microeng.* **15**, 2098 (2005).
5. C. L. Goldsmith, "Temperature variation of actuation voltage in capacitive MEMS switches," *IEEE Microwave Wireless Compon. Lett.* **15**, 718–720 (2005).
6. S. Chen et al., "A new in situ residual stress measurement method for a MEMS thin fixed-fixed beam structure," *J. Microelectromech. Syst.* **11**, 309–316 (2002).
7. J. C. Marshall and D. T. Read, "Analysis of fixed-fixed beam test structures," *Proc. SPIE* **2880**, 46–55 (1996).
8. B. Lakshminarayanan and D. Mercier, "High-reliability miniature RF-MEMS switched capacitors," *IEEE Trans. Microwave Theory Tech.* **56**, 971–981 (2008).
9. R. Stefanini et al., "Miniature MEMS switches for RF applications," *J. Microelectromech. Syst.* **20**, 1324–1335 (2011).
10. M. Song et al., "Design and analysis of a novel low actuation voltage capacitive RF MEMS switches," in *3rd IEEE Int. Conf. on Nano/Micro Engineered and Molecular Systems*, pp. 235–238 (2008).
11. H. D. Espinosa and B. C. Prorok, "A methodology for determining mechanical properties of freestanding thin films and MEMS materials," *J. Mech. Phys. Solids* **51**, 47–67 (2003).
12. C. A. Neugebauer, "Tensile properties of thin, evaporated gold films," *J. Appl. Phys.* **31**, 1096–1101 (1960).
13. C. J. Aguilar-Armenta and S. J. Porter, "Cantilever RF-MEMS for monolithic integration with phased array antennas on a PCB," *Int. J. Electron.* **0**, 1–19 (2015).
14. L. Y. Ma, A. N. Nordin, and N. Soin, "Design, optimization and simulation of a low-voltage shunt capacitive RF-MEMS switch," *Microsyst. Technol.* **21**, 1–13 (2015).
15. G. M. Rebeiz, *RF MEMS: Theory, Design, and Technology*, John Wiley & Sons, Hoboken, New Jersey (2004).
16. C. W. Baek et al., "Measurement of the mechanical properties of electroplated gold thin films using micromachined beam structures," *Sens. Actuators A* **117**, 17–27 (2005).
17. T. C. Hodge, S. A. Bidstrup-Allen, and P. A. Kohl, "Stresses in thin film metallization," *IEEE Trans. Compon. Packag. Manuf. Technol. A* **20**, 241–250 (1997).

Kaan Demirel received the BS degree in physics engineering from Ankara University, in 2006. He was a teaching assistant with the Faculty of Engineering and Natural Sciences at Sabanci University, Istanbul, in 2007–2008. He was a research engineer with the Nanotechnology Research Center and Advanced Research Laboratory, Bilkent University, Ankara, in 2008–2009. He has been a member of the RF MEMS Group at Middle East Technical University since 2009. He is about to graduate with PhD degree in nanotechnology and nanomedicine from Hacettepe University. His research interests include RF MEMS switch design, process development and micro-vacuum devices.

Erdem Yazgan received the BS and MS degrees from the Middle East Technical University, Ankara, Turkey, in 1971 and 1973 respectively, and the PhD degree from Hacettepe University, Ankara, Turkey in 1980, all in Electrical and Electronics Engineering. In 1989 she was a visiting professor with Essex University, Essex, U.K. In 1994–1995, she was with the Electroscience Laboratory, The Ohio State University, Columbus, USA. Between 1990 and 2015, she was a professor at the Department of Electrical and Electronics Engineering, Hacettepe University. She joined the Engineering faculty of TED University as Chair for Electrical-Electronics Engineering in 2015.

Şimşek Demir received the BSc, MSc, and PhD degrees in electrical and electronics engineering from Middle East Technical University (METU), Ankara, Turkey, in 1991, 1993, and 1998, respectively. From 1991 to 1998, he was a research assistant with METU. From 1998 to 1999, he contributed to the atmospheric radar antenna design with IRCTR, TU-Delft, The Netherlands. Since 2000, he has been a Professor with the Electrical and Electronics Engineering Department, METU. He is a recipient of several awards including NATO A2 Fellowship, which supported him as a Visiting Researcher with the University of Massachusetts, Amherst, in 1995.

Tayfun Akın received the BS (Hons.) degree in electrical engineering from Middle East Technical University (METU), Ankara, in 1987, and went to the USA in 1987 for his graduate studies with a graduate fellowship provided by the NATO Science Scholarship Program through the Scientific and Technical Research Council of Turkey. He received the MS and PhD degrees in electrical engineering from the University of Michigan, Ann Arbor, in 1989 and 1994, respectively. Since 1995, 1998, and 2004, he has been an assistant professor, an associate professor, and a professor, respectively, with the Department of Electrical and Electronics Engineering, METU. He is the Director of the METU-Microelectromechanical Systems (MEMS) Center.